Excitonic effect in the optical spectrum of semiconductors

M. del Castillo—Mussot* and L. J. Sham
Department of Physics, University of California, San Diego, La Jolla, California 92093
(Received 1 October 1984)

The electron-hole interaction plays an important role in the optical spectra of semiconductors, not only in bound excitons in the energy-gap region, but also in the continuum. In particular, it affects the strength of the two major peaks in the absorption spectra of semiconductors of diamond and zinc-blende structures. A simple model is made to account for the band-structure effects. The Bethe-Salpeter equation containing the electron-hole interaction effect is solved to yield the absorption spectra for Si and Ge. A physical explanation of how the excitonic effects correct the strength of the E_1 and E_2 peaks in the right direction shows that our conclusions can be generalized to the III-V and II-VI compounds.

I. INTRODUCTION

The typical optical-absorption spectrum of a semiconductor of diamond or zinc-blende structure shows two prominent peaks, known as the E_1 and E_2 peaks.[1–3] These features are qualitatively reproduced by the one-electron band theory, using the noninteracting approximation (NIA), in which the photon is absorbed by an electron, leaving a hole which does not subsequently interact with the electron. In general, the peak positions are not precisely given by theory. However, this is not the problem we wish to address here.

In a broad class of group-VI elemental and III-V, and II-VI compound semiconductors,[4–7] the calculated spectrum within NIA yields an E_1 peak with less strength than measured, but gives an E_2 peak with more strength than the measured peak. These discrepancies have prompted studies of electron-interaction effects on the optical absorption of these materials. These works have been reviewed by Hanke[8] and by Sham.[9] The interaction effects can be separated into local-field effects[10–11] and the excitonic effect. The local-field effect further reduces the main absorption peak in diamond[12,13] and the strength of the E_1 peak in silicon.[14,15] The continuum excitonic effect, i.e., the electron-hole attraction, corrects the strength of the peaks in the correct direction.[13,15] However, in Refs. 13 and 15, the excitonic effect is calculated using local orbital representation. This method, which is appropriate to use in diamond, is difficult to extend to semiconductors of larger atoms such as Ge or GaAs, since it would require an excessive number of overlapping orbitals.

The purpose of this paper is to give a theoretical account of the continuum exciton effect in the optical spectrum which will be valid for this entire class of semiconductors of diamond or zinc-blende structure.[16] To this end, we follow the ideas sketched in the review article by Sham.[9] We employ a simple model which contains the salient features of the band structure and calculate the excitonic effect in the optical spectrum with this model. Evaluation of silicon and germanium shows that the excitonic effect accounts for the discrepancies in the strengths of the E_1 and E_2 peaks. A qualitative understanding of how the oscillator strength shifts the intensity of the spectrum from the E_2 to the E_1 peak emerges from the calculation. This physical picture is general enough to be applied to the III-V and II-VI compounds.

Section II presents a modification of Cardona's model[17] of the one-electron band structure which gives a good account of the optical spectrum within NIA. In Sec. III the energies and wave functions of the model are used to calculate the optical spectra of silicon and germanium in two cases: within the NIA and including the electron-hole attraction. Section IV is devoted to a discussion of the physical picture of the computational results.

II. MODEL FOR THE ELECTRONIC STRUCTURE

A. Nature of the optical peaks

First-principles calculations to date have not been able to reproduce the optical energies accurately. The optical spectrum within NIA is calculated with adjusted energies.[18] Since the emphasis of this work is not to improve the computational accuracy from first principles, but rather to understand the excitonic effect on the absorption peaks, we choose a model for the band structure that is sufficiently simple for computational purposes and which gives a good account of the NIA part of the E_1 and E_2 peaks.

According to Cardona's analysis in NIA,[17] the imaginary part of the dielectric function $\mathrm{Im}\epsilon(\omega)$ of a typical zinc-blende-type or diamond-type semiconductor can be schematized by a three-dimensional critical point at E_0 at low energy, a two-dimensional peak E_1, and a one-dimensional peak E_2. The E_0 feature is due to electronic transitions across the fundamental optical gap at the Γ point (as shown in Fig. 1). The E_1 peak is due to transitions from the neighborhood of the top valence band to the nearly parallel lowest conduction band in the [111] direction, i.e., between the nearly parallel Λ_{3v} and Λ_{1c} bands (Fig. 1). These bands, which are not parallel along the other two perpendicular directions, give the E_1 peak its two-dimensional character. The E_2 peak is due to

transitions in a rather large neighborhood of the X point in the Brillouin zone, (100), between X_{4v} and X_{1c} with bands nearly parallel in two directions (Fig. 1). The one-dimensional character of the E_2 peak arises from the parallel behavior of these two bands along those two directions. The different dimensionality of the E_1 and E_2 peaks explains the stronger peak at E_2 compared to E_1 with NIA and, as will be shown later, plays an important role when the electron-hole attraction, i.e., the excitonic effect, is included in the optical spectrum. A different interpretation for the E_2 peak of Ge is given by Aspnes[19] and Chelikowsky and Cohen.[20] This is discussed in Sec. IV.

B. Band structure around the L point

The E_1 peak in Cardona's model comes from a three-band $\mathbf{k}\cdot\mathbf{p}$ Hamiltonian around the L point, $(\frac{1}{2},\frac{1}{2},\frac{1}{2})$, which yields a two-dimensional optical density of states. The $\mathbf{k}\cdot\mathbf{p}$ method[6] is best suited to account for the fact that the two highest valence bands L_{3v} and the lowest conduction band L_{1c} are parallel along the [111] lines (except near $\mathbf{k}=\mathbf{0}$) because of the absence of $\mathbf{k}\cdot\mathbf{p}$ coupling between these bands for $\mathbf{k}$ along the [111] direction. To show this, we choose the new set of axes (α,β,γ) along $[1\bar{1}0]$, $[11\bar{2}]$, and [111], respectively.

The conduction wave function $\psi_0(L_{1c})$ transforms like γ under the point group which leaves L invariant, while the valence wave functions $\psi_\alpha(L_{3v})$ and $\psi_\beta(L_{3v})$ transforms like (α,β). Under these conditions, the one-particle Hamiltonian (with κ measured from L) is given by

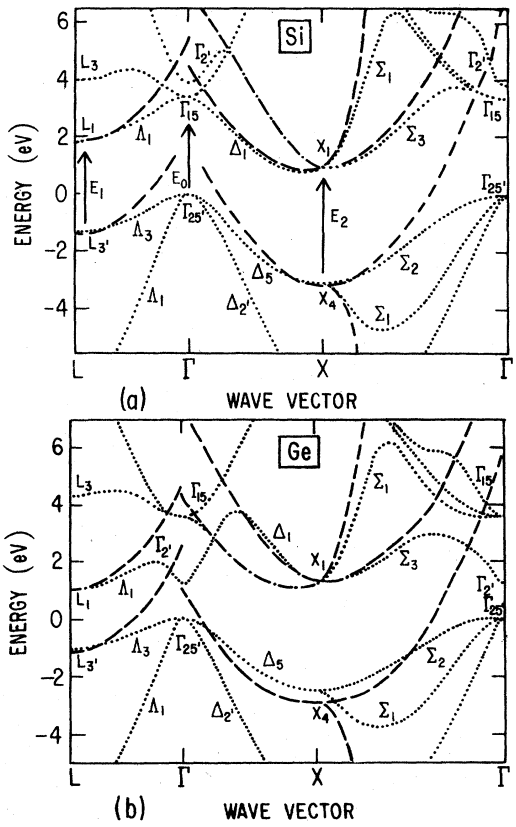

FIG. 1. Band structures of (a) silicon and (b) germanium. In (a) the electronic transitions across the gap responsible for E_0, E_1, and E_2 are indicated by the vertical arrows. Our model band structure (dashed lines) is compared with that of Ref. 21 (dotted lines).

$$\mathcal{H}_L=\begin{bmatrix} E(L_{1c})+\frac{\hbar^2}{2m}\kappa^2 & P\kappa_\alpha & P\kappa_\beta \\ P\kappa_\alpha & E(L_{3v})+\frac{\hbar^2}{2m}(\kappa_\gamma^2-\kappa_\perp^2) & 0 \\ P\kappa_\beta & 0 & E(L_{3v})+\frac{\hbar^2}{2m}(\kappa_\gamma^2-\kappa_\perp^2) \end{bmatrix}, \tag{1}$$

where $\kappa^2=\kappa_\alpha^2+\kappa_\beta^2+\kappa_\gamma^2$, $\kappa_\perp^2=\kappa_\beta^2+\kappa_\alpha^2$, and

$$P=(\hbar/m)\langle\psi_0\,|\,p_\alpha\,|\,\psi_\alpha\rangle=(\hbar/m)\langle\psi_0\,|\,p_\beta\,|\,\psi_\beta\rangle\ . \tag{2}$$

Note that we have replaced $\kappa_\perp^2$ by $-\kappa_\perp^2$ in the second and third diagonal elements of the Hamiltonian [Eq. (1)]. This modification has little effect on the optical energy differences, since the main contribution to the curvature of these bands is due to the coupling of the large matrix element P, but it is made in order to reproduce the downward bending of L of the valence bands along directions normal to [111],[5] as shown by the dashed lines for the band structure of Ge in Fig. 2(b). The resulting eigenvalues for the conduction band c and the valence bands v_1 and v_2 are

$$E_c(\kappa)=\frac{\hbar^2\kappa_\gamma^2}{2m}+\left[\left[\Delta+\frac{\hbar^2\kappa_\perp^2}{2m}\right]^2+p^2\kappa_\perp^2\right]^{1/2}, \tag{3a}$$

$$E_{v_1}(\kappa)=\frac{\hbar^2\kappa_\gamma^2}{2m}-\left[\left[\Delta+\frac{\hbar^2\kappa_\perp^2}{2m}\right]^2+p^2\kappa_\perp^2\right]^{1/2}, \tag{3b}$$

$$E_{v_2}(\kappa)=\frac{\hbar^2\kappa_\gamma^2}{2m}-\left[\Delta+\frac{\hbar^2\kappa_\perp^2}{2m}\right], \tag{3c}$$

where Δ is half of the energy gap at the L point and the energies are measured from the middle of the gap. We use the experimental values of the energy gaps at L listed in Ref. 21. These values are the extrapolations to zero

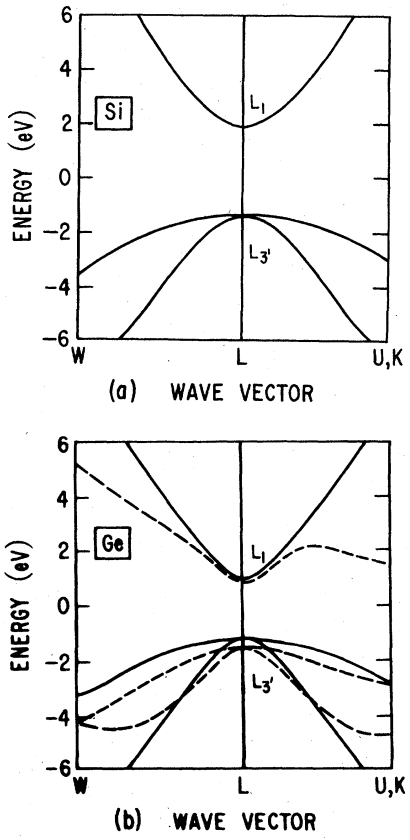

FIG. 2. Band structures for (a) silicon and (b) germanium along symmetry axes in the directions normal to [111]. Only the uppermost valence bands and the lowest conduction band are included. The energy of the conduction band at the L point is fit to that of Ref. 21. In (b) our calculation (solid lines) is compared with that of Ref. 5 (dashed lines).

temperature of the experimental results with the spin-orbit splitting removed. The value of the matrix element P in Eq. (2) is obtained from the transverse effective mass $m_\perp^*$ at L. From Ref. 6, we use the calculated value $m_\perp^*/m=0.130$ for Si and the experimental value[22] $m_\perp^*/m=0.0815$ for Ge. The band structure near L as given by Eqs. (3) is shown in Figs. 1 and 2.

C. Band structure around the X point

The E_2 peak comes from the mixture of six plane waves with wave vectors $(\pm1,\pm1,0)$ and $(0,0,\pm1)$ coupled by the (220)- and (111)-type matrix elements of the pseudopotential[23] around the X point in the extended zone.[17,24] The coupling of the V_{220} component yields a nearly one-dimensional optical density of states with a small splitting along the [100] direction due to the coupling by the V_{111} component.

Analytical expressions for the wave functions and energies of the lowest conduction bands (X_1 symmetry) and of the uppermost valence bands (X_4 symmetry) around the X point are obtained by choosing a basis in which the Hamiltonian matrix is diagonal at the X point and then applying degenerate perturbation theory. The energies are

$$E_{v_1}=E(X_{4v})+\frac{\hbar^2}{2m}(\kappa_\eta^2+\kappa_\xi^2)-A\kappa_\xi^2\,, \tag{4a}$$

$$E_{v_2}=E(X_{4v})+\frac{\hbar^2}{2m}(\kappa_\eta^2+\kappa_\xi^2)-A\kappa_\xi^2\,, \tag{4b}$$

for the valence bands, and

$$E_{c_1,c_2}=E(X_{1c})+\frac{\hbar^2\kappa^2}{2m}+B(\kappa_\zeta^2+\kappa_\xi^2)+C\kappa_\eta^2 \pm\mathrm{sgn}(\kappa_\eta)\{[B(\kappa_\zeta^2-\kappa_\xi^2)]^2+(D\kappa_\eta)^2\}^{1/2}\,, \tag{5}$$

for the conduction bands. For each extended-zone or Jones-zone face, the wave vector $\kappa=(\kappa_\xi,\kappa_\eta,\kappa_\zeta)$ is defined to have its origin at the X point with direction κ_ζ perpendicular to the face, and directions κ_ξ,κ_η along the face.[24] A, B, C, and D are positive coefficients expressible in terms of V_{111} and V_{220} (see Appendix). Along the [100] direction, i.e., $\kappa_\zeta=\kappa_\xi=0$, the valence bands are degenerate and the conduction bands split due to the presence of the term $D\kappa_\eta$, which is zero in the two-plane wave model[9] where V_{111} is neglected. The term $C\kappa_\eta^2$ arising from the next-to-uppermost valence band states is negligible in the neighborhood of X.

The values of V_{220} and V_{111} are adjusted to fit the experimental values[21] of the energy gap, $E(X_{1c})-E(X_{4v})$, and the position of the minimum of the conduction bands along Δ. The position in $\mathbf{k}$ space of the lowest conduction-band minimum in Si is known to be[25] $0.15(2\pi/a)$ as measured from the X point along Δ. For Ge, the value[24] $0.18(2\pi/a)$ is used. The resulting band structures around point X for Si and Ge are shown in Fig. 1, together with the corresponding band structures calculated by Cohen and Bergstresser.[21]

This mixture of a $\mathbf{k}\cdot\mathbf{p}$ model around L and a multiple plane-wave model around X is sufficiently simple for us to calculate the absorption spectrum, both with and without electron-hole interactions, and yet contains important features needed to reproduce the characteristics of E_1 and E_2 peaks.

III. OPTICAL SPECTRA FOR Si AND Ge

A. Noninteracting approximation

To calculate the optical spectra of Si and Ge in terms of the one-particle band structure described in Sec. II, we divide the $\mathbf{k}$ space into two regions in which integrations are performed, Ω_L and Ω_X, centered around the L point and X points, respectively. To facilitate the numerical integration procedure, each of these regions is chosen to be composed of a set of right-angled parallelepipeds. In Ω_L, since our band model of Sec. II B exhibits parallel bands along the [111] direction indefinitely, we restrict integration along γ axis up to the point at which the more accurately calculated conduction and valence bands begin to be significantly not parallel to each other; namely, at a fraction[21] 0.85 for Si and 0.70 for Ge of the distance between L and Γ. Along both α and β axes, integrations are performed around the L point up to a distance equal to half of the segment LU, where our band structure is a good approximation [see Fig. 2(b)]. Around each X point, the

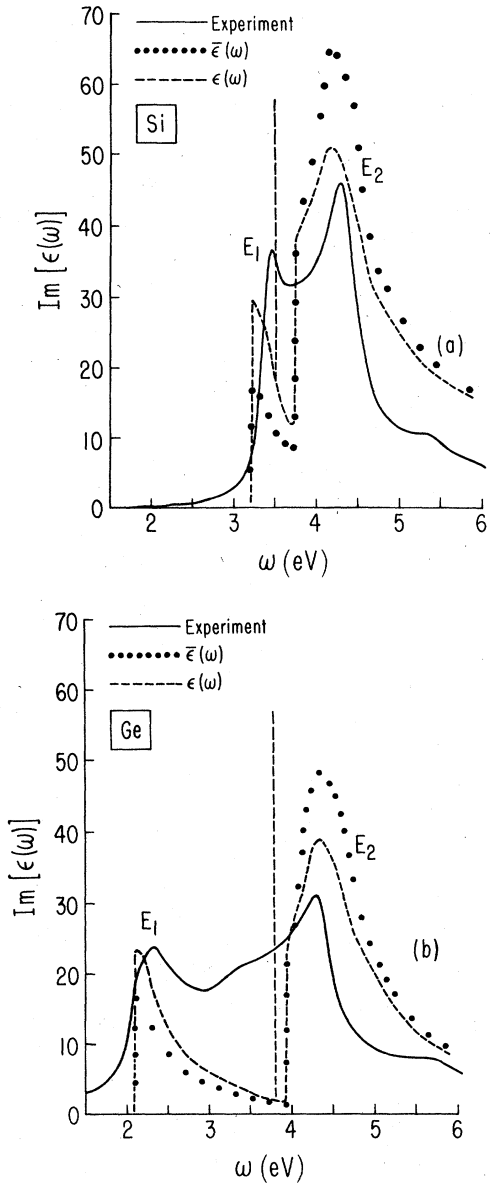

FIG. 3. Absorption spectra Imϵ of (a) silicon and (b) germanium deduced from reflectivity (Ref. 3) and calculated in a simple model without interaction, $\bar{\epsilon}$, and with interaction, ϵ. Interaction between states in Ω_L and those in Ω_X are neglected. The excitonic bound state below the E_2 edge is shown as the δ-function peak.

boundaries of Ω_X are chosen to lie at the midpoint of the segment $X\Gamma$ along the Σ directions and at a quarter of the distance between X and Γ along [100] directions.

The dotted curves in Fig. 3 represent a calculation of the optical spectra of Si and Ge in the NIA in terms of our band-structure model in the regions Ω_L and Ω_X. The abrupt dip between the E_1 and E_2 peaks in the figures marks the boundary between the contributions from the Ω_L and Ω_X regions.

The qualitative features of the E_1 and E_2 peaks due to one-electron theory are reproduced with E_1 weaker than experiment and E_2 much stronger than experiment.

B. Excitonic effects

The electron-hole interaction is included in the optical spectrum in terms of the two-particle Green's function.[15] The equation of motion for this two-particle Green's function S (the Bethe-Salpeter equation) has the form (see Fig. 4)

$$S=S^0+S^0IS\ , \tag{6}$$

where S^0 is the noninteracting electron-hole pair. In S^0, we suppose that the electron and the hole propagators include all of the band-structure effects and the many-body effects on the one-particle state. I is the electron-hole interaction consisting of two parts:[26] I_a, which is the electron-hole attraction, suitably screened, responsible for the excitonic effect; and I_b, which is the bare Coulomb interaction between one electron-hole pair and another, responsible for the local-field effects (see Fig. 5). Close to the E_0 peak, i.e., for the electron transition near the direct fundamental gap, Eq. (6) can be shown to reduce to the effective mass approximation (EMA),[26] which adequately accounts for the bound exciton lines and continuum excitonic effect near E_0,[27] with a small exchange correction.[28] The EMA is, however, invalid around the E_1 and E_2 peaks, since large regions of the phase space contribute to the peaks.

The local-field effect, as produced by including I_b in I, has been calculated for diamond[12,13] and silicon[14,15] in both the plane wave[13,15] and the LCAO representation.[12,14] In both representations, it is found that the local-field effect reduces the intensity of a peak of the optical spectrum in the NIA. In the plane-wave representation, the local-field correction is not very important.

In the following, we include only the excitonic effect in the optical spectra of Si and Ge and keep only the term I_a in I. The Bethe-Salpeter equation can be written as

$$\begin{bmatrix} S_L \\ S_X \end{bmatrix} = \begin{bmatrix} S_L^0 \\ S_X^0 \end{bmatrix} + \begin{bmatrix} S_L^0 I_{LL} & S_L^0 I_{LX} \\ S_X^0 I_{XL} & S_X^0 I_{XX} \end{bmatrix} \begin{bmatrix} S_L \\ S_X \end{bmatrix}\ , \tag{7}$$

where the subscripts to S and I denote the restrictions of the $\mathbf{k}$ vector to the region Ω_L or Ω_X. For $\mathbf{k}$ in Ω_X, the propagators and the interaction-matrix elements are given in terms of the linear combination of plane waves. For $\mathbf{k}$ in Ω_L, they are given in terms of the $\mathbf{k}\cdot\mathbf{p}$ representation with the further approximation in the Coulomb interaction matrix element that the spatial variation of the wave function at L is neglected. In other words, for $\psi_k(\mathbf{r})=F_k(\mathbf{r})\psi_L(\mathbf{r})$, only $F_k(\mathbf{r})$ enters the Coulomb integral.

We use the Penn model[29] for the static dielectric function to screen the Coulomb potential. Since the screened

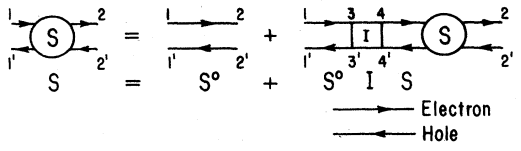

FIG. 4. The Bethe-Salpeter equation.

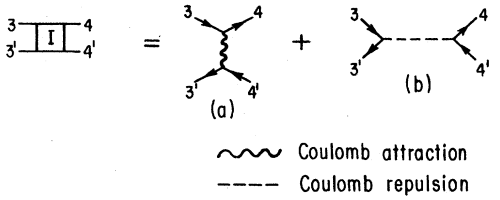

FIG. 5. The irreducible electron-hole interaction I: (a) screened electron-hole attraction; (b) unscreened exchange.

Coulomb attraction is a decreasing function of $\mathbf{q}$, the off-diagonal terms I_{LX} and I_{XL} in Eq. (7) connecting different regions are much smaller than I_{LL} and I_{XX} in the same zones. These small terms are, in the first instance, neglected. Then Eq. (7) is decoupled.

The decoupled integral equation for each region Ω_L or Ω_X contains a logarithmic singularity in the kernel after the angular integration is carried out. The singularity of the kernel comes from the long-range nature of the Coulomb interaction so that $I(\mathbf{k},\mathbf{k}';\omega)$ goes like $1/\epsilon_0 |\mathbf{k}-\mathbf{k}'|^2$ as $\mathbf{k}$ tends to $\mathbf{k}'$. Each integral equation is solved by the "modified quadratic method."[30]

The optical spectra of Si and Ge that include the electron-hole attraction are indicated by the dashed lines in Fig. 3. When compared with the curves in the NIA (indicated by the dotted curves), it is clear that the inclusion of the excitonic effect in our model is an improvement over NIA in the sense that the E_1 peak becomes stronger and the E_2 peak weaker.

No excitonic bound states were found below the edge of the E_1 peak, but for both Si and Ge, the electron-hole states which contribute to the E_2 peaks form a bound state below the E_2 edge that falls in the continuum of states of the E_1 peak. The energies of the bound states are approximately 0.20 eV for Si and 0.08 eV for Ge below the E_2 edge. These δ-function spikes are indicated by dashed vertical lines in Fig. 3.

C. The Fano effect

The bound state created from the states that contribute to the E_2 peak is allowed to interact with the continuum states that contribute to the E_1 peak by reinstating the terms I_{LX} and I_{XL} in Eq. (7). This problem is a particular case of a localized state that is broadened by interaction with a set of continuum states in which it is immersed.[31] The calculated spectra including the interaction between regions Ω_L and Ω_X are shown in Fig. 6, where the broadened excitonic peaks are barely noticeable.

IV. DISCUSSION

In our delocalized description of the electronic wave functions of the covalent semiconductors, we made use of a simple model to calculate the electronic energy-band structure. The essential features of the largest peaks in the optical spectrum, the so-called E_1 and E_2 peaks, are due to absorption from the parallel bands along $L\Gamma$ and around X, respectively. The bands that contribute to the E_1 peak possess the characteristics of two-dimensional

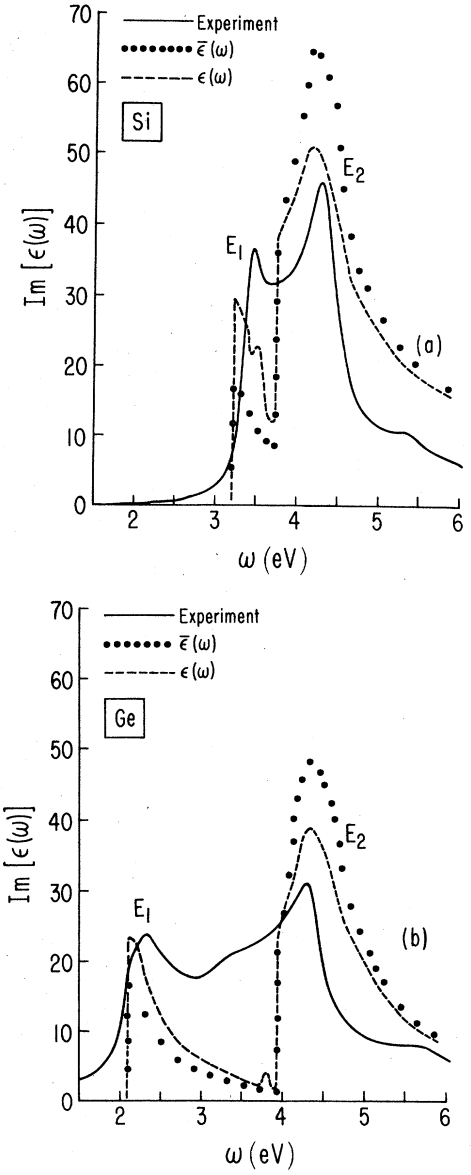

FIG. 6. Same as Fig. 3, but including interaction between states in Ω_X and those in Ω_L.

bands, while the bands that contribute to the E_2 peak have the characteristics of nearly one-dimensional bands. These features are typical of group-IV elemental and III-V and II-VI compound semiconductors.

We find that the attractive interaction between electrons and holes "pulls" the oscillator strength of the E_1 region to lower energy, but above the threshold, thus increasing the E_1 peak height and improving agreement with the measured E_1 peak. Because of the two-dimensional nature of the E_1 peak, the effectively short-range interaction is too weak to form the electron-hole pair into a bound state. The interaction in the E_2 region also pulls the oscillator strength to lower energy but because of the one-dimensional character of the E_2 peak, it now forms a bound state below the E_2 threshold to which

some of the strength is transferred. The electron-hole attraction for the states that contribute to E_1 and E_2 possesses a short-range character due to the large regions of the phase space where it exists. The short-range nature appears to be supported by the experimental work of Pollak and Glembocki.[32]

The mechanism by which the inclusion of the excitonic effect in the simple model increases the height of the E_1 peak and lowers that of the E_2 peak, was explained by Hanke and Sham[15] by invoking the dimensionality of the peaks. Their conclusions were based on Kramers-Kronig analysis of the step function discontinuity of the E_1 peak, and of the inverse square-root singularity of the E_2. The Kramers-Kronig analysis had not included the possibility of bound states below either the E_1 or E_2 edges.

The bound exciton state from E_2 is in the continuum of the E_1 region, and is broadened by the interaction between the electrons in the two regions. This interaction spreads the strength of the excitonic state, as can be seen in Fig. 6, where the resultant resonant state manifests itself as the barely noticeable peaks at 3.51 and 3.78 eV in the calculated optical spectra of Si and Ge, respectively.

As can be seen in Fig. 6, the corrections in the E_1 and E_2 peaks due to the excitonic effects are larger in Si than in Ge. Also the bound state is closer to the E_2 edge in Ge than in Si.

Aspnes[19] observed a well-defined interband reduced mass for the E_2 peak in Ge that suggests a relatively well-localized critical-point origin for this peak. In agreement with this result, Chelikowsky and Cohen[20] conclude from a high-resolution band-structure calculation that the E_2 peak in Ge arises from a well-defined limited region in the Brillouin zone, which is not on symmetry lines, and lies close to the $(\frac{3}{4}, \frac{1}{4}, \frac{1}{4})$ point. This region consists of a nearly, if not completely, degenerate M_1-M_2 pair of critical points. This interpretation is not the same as the quasi-one-dimensional model around the X point,[17] on which our exciton analysis is constructed. It is not clear from the analysis of Aspnes,[19] which comes from the modulation spectroscopy, that the region suggested will provide sufficient strength for the E_2 peak. If the large intensity is produced from this region, the exciton effects may be qualitatively the same as in our model, although we have not investigated the possibility.

We have only computed the absorption spectra for Si and Ge. Since the broad features of the band structure utilized, namely, the dimensionality of the E_1 and E_2 peaks are common to the large family of semiconductors having structures of the zinc-blende type, namely, the III-V and II-VI compounds, our conclusions concerning the continuum excitonic effects on the E_1 and E_2 peaks are equally applicable to this family of semiconductors.

ACKNOWLEDGMENTS

M. del C.-M. gratefully acknowledges the continued financial support of the Universidad Nacional Autónoma de México. One of us (L.J.S.) is supported in part by the National Science Foundation under Grant No. DMR-80-018440 and by the Guggenheim Foundation.

APPENDIX

The coefficients utilized in Eqs. (4) and (5) to describe the one-electron band energies around the X point are expressed in terms of the Fourier components of the pseudopotential, V_{220} (>0) and V_{111} (<0), as follows:

$$A=(8\cos^2\theta/\epsilon_g)-b\ , \tag{A1}$$

$$B=4\cos^2\theta/\epsilon_g\ , \tag{A2}$$

$$C=\sin^2 2\theta/(\epsilon_g+\epsilon_w)\ , \tag{A3}$$

$$D=2\sin^2\theta\ , \tag{A4}$$

where $b=\hbar^2/(2m)$, $\cos 2\theta=d/F$, $\sin 2\theta=-\sqrt{2}V_{111}/F$, $d=(b+V_{220})/2$, $F=(d^2+2V_{111}^2)^{1/2}$, $\epsilon_g=-b+(3V_{220}/2)+F$, and $\epsilon_w=b-(3V_{220}/2)+F$. ϵ_g is the energy gap at X, $E(X_{1c})-E(X_{4v})$, and ϵ_w is the energy difference between the uppermost and the next highest valence bands at X, $E(X_{4v})-E(X_{1v})$.

*Present address: Instituto de Fisica, Apartado Postal 20-364, 01000 México, Distrito Federal, Mexico.

[1]D. L. Greenaway and G. Harbeke, *Optical Properties and Band Structure of Semiconductors* (Pergamon, New York, 1968).

[2]M. Cardona, in *Modulation Spectroscopy,* Suppl. II of *Solid State Physics,* edited by F. Seitz and D. Turnbull (Academic, New York, 1969).

[3]D. E. Aspnes and A. A. Studna, Phys. Rev. B **27**, 985 (1983).

[4]J. L. Freeouf, Phys. Rev. B **7**, 3810 (1973).

[5]W. D. Grobman, D. E. Eastman, and J. L. Freeouf, Phys. Rev. B **12**, 4405 (1975).

[6]M. Cardona and F. Pollak, Phys. Rev. **142**, 530 (1966).

[7]C. W. Higginbotham, F. H. Pollak, and M. Cardona, *Proceedings of the Ninth International Conference on the Physics of Semiconductors, Leningrad, 1967* (Nauka, Leningrad, 1968), p. 57.

[8]W. Hanke, in *Festkörperprobleme (Advances in Solid State Physics),* edited by J. Treusch (Vieweg, Braunschweig, 1979), Vol. 19, p. 1.

[9]L. J. Sham, in *Proceedings of the Fifteenth International Conference on the Physics of Semiconductors, Kyoto, 1980* [J. Phys. Soc. Jpn. Suppl. A **49**, 69 (1980)].

[10]S. L. Adler, Phys. Rev. **126**, 413 (1962).

[11]N. Wiser, Phys. Rev. **129**, 62 (1963).

[12]J. A. Van Vechten and R. M. Martin, Phys. Rev. Lett. **28**, 446 (1972).

[13]W. Hanke and L. J. Sham, Phys. Rev. B **12**, 4501 (1975).

[14]S. G. Louie, J. R. Chelikowsky, and M. L. Cohen, Phys. Rev. Lett. **34**, 155 (1975).

[15]W. Hanke and L. J. Sham, Phys. Rev. Lett. **43**, 380 (1975); Phys. Rev. B **21**, 4656 (1980).

[16]An abbreviated account of this work was included in the Proceedings of the Seventeenth International Conference on the Physics of Semconductors, San Francisco, 1984 (unpub-

lished).
[17]M. Cardona, *Proceedings of the International School of Physics "Enrico Fermi" Course LII, Atomic Structure and Properties of Solids,* edited by E. Burstein (Academic, New York, 1972), p. 514.
[18]J. R. Chelikowsky and M. L. Cohen, Phys. Rev. B **1**, 5095 (1974).
[19]D. E. Aspnes, Phys. Rev. Lett. **31**, 230 (1973).
[20]J. R. Chelikowsky and M. L. Cohen, Phys. Rev. Lett. **31**, 1582 (1973).
[21]M. L. Cohen and T. K. Bergstresser, Phys. Rev. **141**, 789 (1966).
[22]R. W. Levinger and D. R. Frankel, J. Phys. Chem. Solids **20**, 281 (1961).
[23]V. Heine, Phys. Rev. **153**, 673 (1967).
[24]V. Heine and R. O. Jones, J. Phys. C **2**, 719 (1969).
[25]G. Feher, Phys. Rev. **114**, 1219 (1959).
[26]L. J. Sham and T. M. Rice, Phys. Rev. **144**, 807 (1966).
[27]R. J. Elliot, Phys. Rev. **108**, 1384 (1957).
[28]K. Cho, Phys. Rev. B **14**, 4463 (1976).
[29]D. R. Penn, Phys. Rev. **128**, 2093 (1962).
[30]C. T. H. Baker, *The Numerical Treatment of Integral Equations* (Clarendon, Oxford, 1977), p. 193.
[31]U. Fano, Phys. Rev. **124**, 1866 (1961).
[32]F. H. Pollak and O. J. Glembocki, Bull. Am. Phys. Soc. **27**, 142 (1982).